arXiv:astro-ph/0111125v1 6 Nov 2001

The Lyman–α forest of a Lyman Break Galaxy: VLT Spectra of MS1512–cB58 at $z = 2.724$[1]

S. Savaglio[2]
Osservatorio Astronomico di Roma, Via di Frascati 33, I–00040 Monteporzio, Italy

N. Panagia and P. Padovani[3]
Space Telescope Science Institute, 3700 San Martin Drive, Baltimore, MD21218, USA
On assignment from the Space Science Department of the European Space Agency

ABSTRACT

The high redshift galaxy MS1512–cB58 ($z = 2.724$, $m_V = 20.64$) has been observed with the very efficient high resolution echelle spectrograph VLT/UVES. Although this is a very challenging observational program for a Southern hemisphere telescope (the galaxy is located at $+36°$ declination), high resolution spectra (FWHM $\simeq$ 26 km s^{-1}) have revealed, with unprecedented detail along a galaxy sight line, the Lyman–α forest due to intervening clouds in the intergalactic medium (IGM). The mean depression D_A due to IGM absorption blueward of the galaxy Lyα wavelength and the number density dn/dz of Lyα clouds have been compared with equivalent results obtained for QSO sight lines at similar redshifts. Our results indicate a possible excess of absorption close to the galaxy. The mean depression at $\sim 150\ h_{65}^{-1}$ Mpc comoving ($\Omega_m = 0.3$, $\Omega_\Lambda = 0.7$) from the galaxy is $D_A = 0.36 \pm 0.03$, to be compared with 0.22 ± 0.04, expected from a best fit to QSO sight lines. In the same region ($z \simeq 2.610$), the number density of lines with HI column density in excess of 10^{14} atoms cm^{-2} is also $\sim 3\sigma$ larger than expected. This high density region is at least $60\ h_{65}^{-1}$ Mpc comoving wide, but the large Lyα absorption of the galaxy itself prevents us from detecting a possible structure extending down to the galaxy.

This excess of Lyα clouds is suggestive of two possible scenarios. One is the presence of a super cluster of Lyα clouds not associated with cB58. The other is a high density of gas associated with the environment of cB58. Indeed, a hint of

[1]Based on observations collected at the European Southern Observatory, the VLT/Kueyen telescope, ESO, Paranal, Chile (ESO Programme 65.O-0471).

[2]Present address: The Johns Hopkins University, 3400 North Charles Street, Baltimore, MD21218, USA

[3]On leave of absence from Dipartimento di Fisica, II Università di Roma "Tor Vergata", Italy

the complexity of cB58 and possibly its environment is given by the huge velocity range (almost 1000 km s^{-1}) between the optical emission of star forming regions and UV absorption of its interstellar medium.

Subject headings: cosmology: observations – galaxies: Lyα forest – galaxies: individual MS1512–cB58

1. INTRODUCTION

Lyman break galaxies (LBGs) are by definition characterized by a strong absorption longward of the Lyα wavelength due to intervening intergalactic gas and intrinsic UV emission of strong star formation, and so can easily be found using the color–color technique (Steidel et al., 1996). This technique is efficient for redshifts larger than 2, where intergalactic absorption is more pronounced and the galaxy UV flux is redshifted to the optical, allowing observations from the ground.

The rest frame UV spectrum of a galaxy bears the signature of its interstellar medium through absorption lines and stellar activity through line and broad band emission. Although low resolution UV spectra of galaxies are available for the local universe, high resolution data are strongly limited by the low efficiency of space telescopes. Only recently the far UV spectrograph (FUSE) started to deliver high resolution (HR, $R \sim 10,000$) spectra of nearby star forming galaxies, revealing for the first time complex structures (Heckman et al., 2001).

In principle, high redshift galaxies can benefit of the fact that their UV emission is redshifted to the optical and can, therefore, be studied by large ground-based telescopes. However, their apparent optical magnitude is generally fainter than $\sim$ 23 and HR spectroscopy cannot be performed. Other possible candidates for HR spectroscopy are the very powerful radio galaxies, but no radio galaxy at redshift larger than $z = 1.5$ and brighter than $m \sim 21$ has been found so far. This limit is just a little beyond the HR capabilities of the largest telescopes.

The chance to observe high redshift galaxies at high spectral resolution is then confined to gravitational lensed galaxies and gamma ray burst (GRB) afterglows. The latter are indeed potentially very interesting for future observations (Fiore et al., 2000) thanks to the advent of new X–ray satellites (HETE2 and in the near future SWIFT) that are capable of prompt identification of GRBs. The former are still penalized by a limited number of sufficiently bright targets. A unique case is the galaxy MS1512–cB58 ($z = 2.724$).

This very bright gravitational lens LBG ($m_V = 20.65$, Ellingson et al., 1996) is within the state of the art capabilities of HR spectrographs of the largest ground based telescopes. It was serendipitously discovered by Yee et al. (1996) during the CNOC cluster redshift survey and is gravitationally lensed by the cluster MS1512+36 at $z = 0.37$ (Seizt et al. 1998). The gravitational magnification has been studied in detail by Seitz et al. (1998) who found that the 2×0.2 arcsec^2 arclet brightness is amplified ~ 50 times by the cD galaxy of the cluster, $6''$ apart. Since this is the brightest LBG galaxy known, it has been widely studied in the optical, submillimeter and radio bands, both in imaging and spectroscopy. Optical low resolution spectra obtained with Keck/LIRIS (Pettini et al., 2000) showed the complex structure of the interstellar medium of the galaxy.

Observations of cB58 were performed using the UV–visual Echelle Spectrograph (UVES) of the ESO Very Large Telescope (VLT). This instrument/telescope combination is the best possible today for Lyα forest observations. The main motivation of the program was to investigate the intervening absorption and compare its properties with the equivalent in QSO forests. The results of the analysis of the intergalactic Lyα forest distributed along the cB58 sight line are presented in this paper. The second goal was the study of the metallicity and dust content in the interstellar medium of the galaxy itself. These results will be presented in a future paper.

2. OBSERVATIONS AND DATA REDUCTION

The galaxy MS1512–cB58 ($\alpha = 15^h14^m22.2^s$ $\delta = +36°36'24''$, J2000) was observed with the high resolution UV–visual echelle spectrograph (UVES, Dekker et al., 2000) mounted at the UT2 telescope of the VLT observatory, at Paranal (Chile). The program was run in Service Observing mode between March and August 2000. The log of the observations is shown in Table 1. The red and blue arms of UVES were used, centered at $\lambda = 5200$ Å and 4370 Å, respectively. Due to the high declination of the object with respect to the latitude of the VLT observatory ($-24°40'$), the observations were performed in chunks of ~ 1.5 hours around the meridian ($\sim 29°$ above the horizon) to minimize atmospheric absorption. Indeed, the airmass ranged between 2.1, the minimum value for this object observed from Paranal, and 2.3. In order to maximize the signal–to–noise ratio (S/N), the CCD was rebinned 2×2 pixels during observations. Due to good seeing conditions, the slit aperture was always set to $1'' \times 9''$ and $1'' \times 10''$ for the Red and Blue arm set–ups, respectively, and its inclination was along the galaxy apparent major axis.

The data reduction has been performed using a MIDAS package specifically implemented for UVES data. The final useful spectral coverage was $\lambda\lambda = 4150 - 5000$ Å for the blue

arm, and $\lambda\lambda = 4500 - 5164$ Å and $\lambda\lambda = 5241 - 6206$ Å for the red arm. The pixel size was set to a constant value of 0.2 Å in the final combined spectrum. The final resolution element corresponding to two pixels then ranges from FWHM = 29 km s^{-1} at 4150 Å, to 26 km s^{-1} at the Lyα, to 19 km s^{-1} at 6206 Å. The noise spectrum, used to determine the errors on the line parameters, has been calculated through photon statistics propagation of object and sky spectra and the detector read–out–noise. The final S/N ratio per resolution element is S/N$\simeq$ 3 at $\lambda = 4150$ Å, S/N$\simeq$ 7 at $\lambda = 4550$ Å, S/N$\simeq$ 8 at $\lambda = 5500$ Å, and S/N $\simeq$ 10 at $\lambda = 6100$ Å.

The fit to the continuum blueward of the galaxy Lyα was performed interpolating between points of the observed flux free of apparent absorption. Although this is not particularly easy due to the non–excellent S/N ratio of the spectrum, at these redshifts the line density of Lyα clouds allows the detection of several regions that are most likely unabsorbed. The final normalized galaxy and noise per resolution element spectra in the interval $\lambda\lambda = 4150 - 4595$ Å are shown in Fig. 1.

3. THE LYMAN ALPHA FOREST OF cB58

The magnification of cB58 and the excellent performance of UVES make this galaxy the only suitable candidate today to study the intergalactic matter distributed along a galaxy sight line, similarly to what is normally done for QSO sight lines. The study of QSO Lyα forests has led in the past to a broad understanding of the formation and evolution of the Universe. Very briefly we mention successful experiments to test the intergalactic medium (IGM) reionization through the Gunn–Peterson effect for HI and HeII, the early metal pollution of the IGM, and the intensity of the UV background radiation, as discussed by Songaila (1998), Songaila et al. (1999), Heap et al. (2000), Ellison et al. (2000), just to mention the most recent publications on these subjects.

For the first time we can test some of these results considering a galaxy line of sight. Any deviation from the expected properties of the IGM might be strongly connected to a deviation of the galaxy surrounding environment with respect to the QSO ones. To study the cloud distribution in cB58, we have performed line fitting with Voigt profiles using the MIDAS package FITLYMAN (Fontana & Ballester, 1985). The wavelength range considered here is $\lambda\lambda = 4150 - 4550$ Å. The upper limit is set by the wavelength of the galaxy Lyα line. Fig. 1 shows the Lyα forest of cB58, together with the fitted absorption profiles. In this range some metal lines associated with cB58 itself have been identified and fitted for completeness. No other metal lines associated with intervening metal systems at $z = 0.828$ and 1.339 reported by Pettini et al. (2000), and at $z = 2.007$, 2.117 and 2.660 identified by us, have

been found in this interval.

In Table 2 we report absorption line parameters for the Lyα lines only, namely the redshift z, column density $N_{\rm HI}$, and the Doppler parameter b.

The intrinsic spectrum of the galaxy shows a very large Lyα absorption that extends almost 100 Å in the range $\lambda\lambda \simeq 4480 - 4570$ Å. This large trough has been considered by Pettini et al. (2000) as a single interstellar cloud at $z = 2.7240$ with an HI column density of $N_{\rm HI} = 7.5 \times 10^{20}$ cm^{-2}, assuming that the peak around 4540 Å is due to Lyα emission of cB58 redshifted to $z = 2.7326$ ($v = +690$ km s^{-1}). Making the same assumption we find a slightly lower HI content, but still consistent with Pettini et al.'s result, with $N_{\rm HI} = 6^{+1.4}_{-2} \times 10^{20}$ cm^{-2} and redshift $z = 2.72417$. However we also notice that in our spectrum the core of this Lyα absorption ($\lambda\lambda = 4520 - 4535$ Å) is not completely black, and a small residual mean flux of about 1σ above the zero level is present. This might indicate that the interstellar clouds are not fully covering the star forming regions of the galaxy and/or that resonant scattering fills up part of the absorption.

Other metal lines associated with cB58 are listed in Table 3. Due to the large HI absorption and metal lines associated with the galaxy, we have considered in our analysis the Lyα forest shortward of $\lambda = 4430$ Å, namely, the redshift range $2.4137 \leq z \leq 2.6441$ ($\Delta z = 0.23$). Since the galaxy intrinsic brightness is much lower than a typical distant QSO, the classical proximity effect, that in a QSO decreases the cloud density within ~ 8 Mpc from the source due to the high QSO UV ionizing flux, is in the case of cB58 negligible. Indeed, taking the observed magnitude and magnification, the absolute magnitude of the galaxy is $M_B \sim -22$, that is several hundreds times fainter than a high redshift QSO typically used for proximity effect studies. For instance, if we compare cB58 with a QSO 400 times brighter, the ionization region is 20 times smaller. This is even smaller if we consider that the spectrum of a galaxy is much softer than that of a QSO and that the intensity of UV ionizing spectrum is much weaker. We conclude that the proximity distance for cB58 is confined to within 1 Mpc from the galaxy center. The upper redshift limit of $z = 2.6441$ corresponds to a comoving distance from the galaxy of about 90 h_{65}^{-1} Mpc (we adopt throughout the paper a flat Universe with non-zero cosmological constant: $\Omega_m = 0.3$ and $\Omega_\lambda = 0.7$). In the following sections we discuss how an excess of Lyα clouds can be present if the galaxy is embedded in a rich environment which might be typical for a star forming high redshift galaxy.

To make a comparison with mean absorption in QSO sight lines, we have considered two approaches: *i*) we have measured the mean flux depression blueward of the cB58 Lyα line (D_A) and *ii*) we calculated the number density of Lyα clouds.

3.1. Mean flux depression in cB58

The mean flux depression D_A overcomes the problem of moderate signal–to–noise ratio in the spectrum. It is defined by the equation:

$$D_A \equiv 1 - \langle f_{obs}/f_{int} \rangle \tag{1}$$

where f_{obs} and f_{int} are the observed and intrinsic galaxy fluxes, respectively, in the Lyα forest between the rest frame Lyα and Lyβ wavelengths. This quantity is also expressed in terms of the effective optical depth in the same region:

$$D_A \equiv 1 - e^{-\tau_{\rm eff}} \tag{2}$$

and has been measured in the past in QSO sight lines when the data quality did not allow an accurate column density determination of absorption lines (e.g, Giallongo & Cristiani, 1990). More recently Fardal et al. (1998) have computed D_A using different models of intergalactic absorption and compared results with observations. The observed points are obtained not directly from the spectra, but from line lists of Keck data and other lower S/N data. Their Fig. 3 gives $D_A \sim 0.1$ at $z \sim 2.25$ and $D_A \sim 0.25$ at $z \sim 2.8$. In an extensive study of the mean HI opacity in QSOs, Kim et al. (2001a) report $\tau_{\rm eff}$ values in 13 QSOs observed with VLT/UVES and Keck/HIRES and give a best fit to the data in the interval $1.6 < z < 4.3$ as $\tau_{\rm eff} = (0.0030 \pm 0.0008)(1+z)^{3.43\pm0.17}$.

In our analysis, we considered the few very recent high resolution spectra of QSO sight lines observed at similar redshifts, e.g. the Keck/HIRES spectra of GB1759+7539 ($z_{em} = 3.05$; Outram et al., 1999), and HS1946+7658 ($z_{em} = 3.051$; Kirkman & Tytler, 1997), and the VLT/UVES spectra of HE1347–2457 ($z_{em} = 2.534$; Kim et al., 2001b) and J2233–606 ($z_{em} = 2.238$; Cristiani & D'Odorico, 2001) obtained during the science verification of the instrument. Details of the QSO spectra used are given in Table 4, while in Fig. 2 we show the Lyα forest of cB58 and the comparison with QSOs in the region of overlapping (except for J2233–606 that is too blue for cB58). For all the four QSO spectra, we have excluded the proximity effect region. For GB1759+7539, we have calculated the mean depression redward of the QSO Lyβ emission and far from the proximity effect and from a large HI absorption due to an intervening damped Lyα system at $z = 2.626$. For HE1347–2457 we have considered the region 4050 Å $< \lambda <$ 4250 Å. For J2233–606 we have excluded the region with two strong HI absorptions ($N_{\rm HI} > 10^{16}$ atoms cm^{-2}) associated with two metal systems at $z < 1.943$.

For cB58 we have calculate D_A in the range 4150 Å $< \lambda <$ 4430 Å, corresponding to

$2.4137 < z < 2.6441$. For the uncertainties on the mean depression, we have re–calculated D_A considering as a new continuum the original estimate ±5% for cB58, GB1759+7539 and J2233–606, and ±3% for HE1347–2457 and HS1946+7658, respectively, according to S/N. We take as our error the uncertainty derived according to this procedure. The value of D_A in the whole cB58 interval at $\langle z \rangle = 2.5289$ is $D_A = 0.263 \pm 0.037$. This is consistent with the value calculated from the model of the fitted Voigt profiles listed in Table 2, i.e. $D_A = 0.255$. The total mean depression D_A in the QSOs is given in Table 4, while in Table 5 we report D_A in different redshift intervals for cB58 and the QSOs, with the error range between brackets. These values of D_A have been combined with results for other QSOs given by Kim et al. (2001a) and reported, as a function of redshift, in Fig. 3.

Considering the uncertainty and the cosmic variance that we expect in different lines of sight, we can conclude that the D_A values for cB58 are consistent with those for QSOs in the first two redshift bins. However, we notice that the mean depression in cB58 is appreciably larger than expected from QSOs in the last redshift bin. In the last redshift bin of cB58 we have $D_A = 0.36 \pm 0.03$ at $\langle z \rangle = 2.6104$, while the best fit to QSO sight lines gives $D_A = 0.22 \pm 0.04$ at the same redshift (Kim et al., 2001a), a $\sim 3\sigma$ effect.

We notice that metal lines associated with cB58 could contribute to D_A. This effect is marginally important in QSO sight lines, because the powerful UV emission of QSOs highly ionize the foreground gas of the host galaxy. To verify what this contribution is in cB58, we have compared its UV spectrum with the UV spectrum of a nearby galaxy. Thanks to the advent of FUSE, it is now possible to get high resolution UV spectra of galaxies. One example is presented by Heckman et al. (2001), who discuss the OVI outflow in the dwarf starburst galaxy NGC1705. In Fig. 4 we compare their FWHM = 30 km s^{-1} resolution spectrum with that of cB58 in the region of overlapping. The rest frame overlapping range $\lambda\lambda = 1110 - 1183$ Å corresponds for cB58 to the observed interval $\lambda\lambda = 4134 - 4405$ Å. The rest frame of cB58 is calculated assuming a redshift of $z = 2.7244$, that is the redshift of the strongest central absorbing cloud in its interstellar medium (ISM). The absorption lines in NGC1705 show different contributions coming from the ISM and high velocity clouds of the Milky Way, and the ISM of NGC1705 itself, spanning a total velocity range of about 600 km s^{-1} (Heckman et al., 2001). The strongest interstellar lines in NGC1705, FeIIλ1144 or NIλ1134, are also identified in cB58. However, the involved column densities are about an order of magnitudes higher in cB58. The strong absorption on the blue side of the FeII complex, on the other hand, is due to the Galactic ISM, where metallicity and column densities are much larger.

The strong SiIV absorption doublet at $\lambda\lambda = 1122, 1128$ Å and the CIII absorption line at $\lambda = 1176$ Å in the spectrum NGC1705 are due to OB stars (Walborn & Bohlin, 1996).

In cB58 the absorption at $\lambda \sim 4383$ Å can be identified with CIII absorption redshifted by about 300 km s^{-1} with respect to the ISM. The fitted profile shown in Fig. 1 has been obtained assuming a width of 250 km s^{-1} for this line, very similar to what observed for NGC1705. The contribution of the SiIV doublet in cB58 seems to be not very significant (the first component is basically absent, while the second one is very weak). From unpublished HST/STIS high resolution data of NGC1705 (Heckman, private communication) we have seen that there are no other strong absorptions longward of the CIII feature in NGC1705, up to $\lambda \simeq 1189$ Å, corresponding to $\lambda \sim 4430$ Å in the cB58 observed frame, so other further contributions to D_A caused by the cB58 ISM can be considered negligible.

We have then recalculated D_A in the last wavelength bin of the cB58 forest and excluded CIII absorption around $\lambda \sim 4383$ and found $D_A = 0.336 \pm 0.033$. This is still significantly larger than what found in QSOs and supports the idea that the excess of absorption at $z \sim 2.61$ (150 h_{65}^{-1} Mpc comoving from the galaxy) is not due to the galaxy itself but is associated with the intervening intergalactic matter.

3.2. Number density of Lyα clouds in cB58

The next comparison between LBG and QSO forests is through the number density per unit redshift of Lyα clouds with HI column density higher than a threshold N_{th}. This eliminates the problem of the metal lines associated with cB58. The number density per unit redshift is parameterized as $dn/dz \propto (1+z)^{\gamma}$. For a non–evolving population in the standard Friedmann universe with null cosmological constant, $\gamma = 1$ and 0.5 for $q_o = 0.0$ and 0.5, respectively, whereas a non–evolving slope can be approximated by $\gamma \sim 0.7$ for a non-zero cosmological constant universe (Kim et al., 2001a). Recent work on QSO sight lines at different redshifts has shown that strong Lyα clouds ($N_{\rm HI} > 10^{14}$ atoms cm^{-2}) evolve at high redshift ($\gamma \sim 2$ for $z > 1.5$, Kim et al., 2001a) followed by a flat distribution at redshifts $z < 1.5$ ($\gamma \simeq 0.16$, HST key program, Weymann et al., 1998; Penton et al., 2000) consistent with no evolution. Tracking the number density evolution has implied a comparison of low resolution with high resolution data. This complicates the interpretation; however, the results are quite striking.

The number density evolution is different for different N_{th}, being flatter at smaller N_{th} for the large z range (Penton et al., 2000, Kim et al., 2001a). In cB58 we have calculated dn/dz dividing the redshift interval in three different redshift bins as done in the previous section to calculate D_A. We also consider two different N_{th}, namely, $10^{13.7}$ and $10^{14.0}$ atoms cm^{-2}. This is because the completeness of the Lyα sample varies along the spectrum of cB58. Indeed, the 4σ completeness of HI column densities obtained from Lyα lines with Doppler

parameter in the range 20 km s^{-1} $< b <$ 40 km s^{-1}, is $N_{\rm HI} = 10^{13.5}, 10^{13.7}$, and $10^{14.0}$ atoms cm^{-2} for $\lambda > 4270, 4180$, and 4150 Å, respectively. The limited resolution and S/N have the consequence of underestimating the number of components observed in the absorption profile and overestimating the HI column density. In other words, for low or high N_{th}, the number of detected clouds is underestimated or overestimated, respectively. In Tables 6 and 7 we report the number of clouds with $\log N_{th} = 13.7$ and 14.0, while in Fig. 5 we show the number density evolution as a function of redshift for clouds with $N_{th} \geq 10^{14}$ cm^{-2}. When considering results for $\log N_{th} = 14.0$ one should take into account that the number of Lyα clouds might be overestimated if blending of lines is important. However, this is unlikely to have a major effect on our sight line, given the relative sparseness of Lyα lines at these redshifts. In the same tables, we also make a comparison with the Lyα forests of GB1759+7539, HE1347–2457 and HS1946+7658. Between brackets we give the 1σ range obtained using Poisson statistics (Gehrels 1986). As typically done for QSO forests, the identified metal lines in cB58 and in the QSOs associated with the galaxy itself or other metal systems along the line of sight have been excluded from the counting.

Tables 6 and 7 show that there is consistency in the number of Lyα clouds between cB58 and QSO forests in the first two redshift bins, whereas we find again a significant discrepancy when the last redshift bin is considered. This deviation appears more clearly in Fig. 5 for Lyα clouds with HI column density larger than 10^{14} atoms cm^{-2} and is at the 2.7σ level with respect to the best fit to QSO forests in the interval $2 < z < 4$.

As already found in the previous section where the mean depression is considered, the number density of Lyα clouds gives a hint of an excess of gas absorption in cB58 with respect to QSOs at $z \simeq 2.61$, or in the region within 150 h_{65}^{-1} Mpc from the galaxy. This excess appears to be more concentrated in the wavelength range $\lambda\lambda = 4370 - 4430$, at a mean redshift of $\langle z \rangle = 2.6194$. If this structure is isolated and not associated with the galaxy itself, it is ~ 60 h_{65}^{-1} Mpc comoving wide (velocity width of ~ 4000 km s^{-1}).

4. DISCUSSION

Observations of the Lyα forest have been fundamental in helping to unveil the nature of the intergalactic gas. These studies have been possible using large collecting areas pointed on very bright sources. The only suitable candidates so far have been bright ($m_V < 19$), distant ($z > 2$) QSOs, observed with 4m and 10m class ground based telescopes. Similar studies are still precluded if normal Lyman Break Galaxies or radio galaxies are considered. This is because no high-redshift galaxy brighter than $V \sim 21$ is known. A unique chance has been offered to us by VLT/UVES observations of the LBG galaxy cB58. This galaxy

at $z = 2.724$ is gravitationally magnified ~ 50 times by an intervening galaxy cluster at $z = 0.37$ and its optical apparent magnitude is $m_V = 20.64$. This is by far the brightest LBG known.

We have for the first time explored the Lyα forest of a high redshift galaxy and compared the observed properties with those shown by QSO sight lines. We found in cB58 an excess of absorption at a distance from cB58 ($z = 2.724$) of about 150 h_{65}^{-1} Mpc comoving ($z \simeq 2.61$). This has been quantified by both measuring the mean flux depression D_A due to HI absorption and the number density of Lyα clouds with $N_{\rm HI} > 10^{14}$ atoms cm^{-2}. The deviation is in both cases significant at the $\sim 3\sigma$ level. The large Lyα absorption and some metal lines associated with cB58 prevent us to detect Lyα intervening clouds for redshift larger than $z = 2.644$, so we cannot exclude the possibility that this high density region is more extended. We now have two possible scenarios, depending on the size of the region associated with this excess.

1) The excess is due to the presence of a super cluster of Lyα clouds not associated with cB58. This super cluster of lines appears to be concentrated at $2.5947 < z < 2.6441$ ($\Delta z \sim 0.05$), corresponding to a region $\sim 60\ h_{65}^{-1}$ Mpc comoving wide. This is an interesting possibility in view of the fact that a very large structure on scales $\Delta z \sim 0.1$ or $\sim 100\ h_{65}^{-1}$ Mpc has been found at $z \sim 3.1$ in the LBG galaxy distribution (Steidel et al., 1998). Steidel et al. also suggest that similar clustering is common in LBG surveys and that LBGs represent the progenitors of local massive galaxies.

2) The excess is due to high-density gas associated with the environment of cB58. In this case, this high density region could extend all the way down to the galaxy. This has interesting implications for the proximity effect. The proximity effect is used to measure the intensity of the UV background radiation, assuming that the gas distribution of the IGM is independent of the distance from QSOs. Our findings seem to undermine this assumption, which has also been questioned by Pascarelle et al. (2001), using a completely different approach. These authors have analyzed the clustering properties of galaxies and QSO absorption line pairs at low redshifts ($z \lesssim 1$) and found that galaxies and Lyα clouds cluster around QSOs. This effect extends up to a velocity range from the QSO of $\Delta v \sim 3000$ km s^{-1}. In cB58 the clustering would be extended down to $z \sim 2.61$ ($\Delta z \sim 0.11$), corresponding to a velocity range of $\sim 10,000$ km s^{-1}. We can imagine that a clustering effect similar to that found by Pascarelle et al. (2001) may occur in star forming Lyman break galaxies, such as cB58. Indeed, its rest frame optical emission lines give an amplified star formation rate (SFR) of 620 M$_\odot$ per year (Teplitz et al., 2000), which becomes ~ 10 M$_\odot$ per year if corrected by the amplification factor of ~ 50. If cB58 is a starburst galaxy, as suggested by its SFR, then a large density of starforming galaxies is expected in its environment, and therefore a

large number of absorbing clouds as well, consistent with our findings. Further evidence of the peculiarity of cB58 is given by the large velocity range shown by its components: the ISM absorption ($z = 2.7244$) and the emission lines ($z = 2.7290$) are spread over almost 1000 km s^{-1}.

If the excess found around cB58 is typical in collapsed objects, the QSO proximity effect has been underestimated so far and therefore the intensity of the UV background is overestimated. This, in turn, has important implications for estimates of the contribution of the Lyman–α forest to the barionic content of the Universe.

To assess the general validity of our results in other LBG forests, it is necessary to analyze other good quality LBG spectra. This relies on the chance that other gravitationally lensed LBGs are discovered, hopefully with a magnification factor larger than that of cB58. An alternative solution to study the intrinsic properties of high redshift galaxies and the intervening IGM clouds can be provided by GRB afterglow observations. GRB afterglows have been found up to redshifts of 4.5 and their optical magnitude can be as bright as 15^{th} magnitude. These are perfect candidates for high resolution spectroscopy, provided that they are promptly targeted soon after the burst.

The authors wish to thank Tim Heckman, Tea–Sun Kim, David Kirkman, Phil Outram and David Tytler for providing spectra and Lyα forest lists. We are also grateful to our referee, David Kirkman, for very insightful comments, and Tim Heckman for helpful discussions. SS acknowledges the support of the ESO and STScI Visitor Programs. SS would like to express her gratitude for warm hospitality at ESO Garching where the data reduction of UVES spectra has been performed. Special thanks to Vanessa Hill, Andrea Modigliani, Stefano Cristiani and Sandro D'Odorico for helping with the UVES pipeline. The Paranal and UVES teams are acknowledged for their effective support with observations.

REFERENCES

Cristiani S., D'Odorico V., 2000, AJ, 120, 1648

Dekker H., D'Odorico S., Kaufer A., Delabre B., Kotzlowski H, 2000, The International Society for Optical Engineering, 4008, 534

Ellingson E., Yee H. K. C., Bechtold J., Elston R., 1996, ApJ, 466, L71

Ellison S. L., Songaila A., Schaye J., Pettini M, 2000, 120, 117

Fiore F., Nicastro F., Savaglio S., Stella L., Vietri M., 2000, ApJ, 533, L7

Fontana A., Ballester P., 1995, The ESO Messenger, 80, 37

Gehrels N., 1986, ApJ, 303, 336

Giallongo, E., Cristiani, S., D'Odorico, S., Fontana, A., Savaglio, S. 1996, ApJ, 466, 46

Heap S. R., Williger G. M., Smette A., Hubeny I., Sahu M. S., Jenkins E. B., Tripp T. M., Winkler J. N., 2000, ApJ, 534, 69

Heckman T. M., Sembach K. R., Meurer G. R., Strickland D. K., Martin C. L., Calzetti D., Leitherer C., 2001, ApJ, 554, 1021

Hu E. M., Kim T.-S., Cowie L. L., Songaila A., Rauch, M., 1995, AJ, 110, 1526

Kim T.–S., Carswell R. F., Cristiani S., D'Odorico S., Giallongo E., 2001b, MNRAS, submitted

Kim T.–S., Cristiani S., D'Odorico S., 2001a, A&A, 373, 757

Kirkman, D., Tytler, D., 1997, AJ, 484, 672

Lu L., Sargent W. L. W., Womble D. S., Takada–Hidai M., 1996, ApJ, 472, 509

Outram P. J., Chafee F. H., Carswell R. F., 1999, MNRAS, 310, 289

Pascarelle S. M., Lanzetta K. M., Chen H–W, Webb J. K., 2001, ApJ, in press, astro–ph/0107295

Penton P. J., Shull J. M., Stocke J. T., 2000, ApJ, 544, 150

Pettini M., Steidel C. C., Adelberger K. L., Dickinson M., Giavalisco M., 2000, ApJ, 528, 96

Savaglio S., et al., 1999, 515, L5

Steidel C. C., Adelberger K. L., Dickinson M., Giavalisco M., Pettini M., Kellogg M., 1998, ApJ, 492, 428

Steidel C. C., Giavalisco M., Pettini M., Dickinson M., Adelberger K. L., 1996, ApJ, 426, L17

Seitz S., Saglia R. P., Bender R., Hopp U., Belloni P., Ziegler B., 1998, MNRAS, 298, 945

Songaila A., 1998, AJ, 115, 2184

Songaila A., Hu E. M., Cowie L. L., McMahon R. G., ApJ, 525, L5

Teplitz H. I., McLean I. S., Becklin E. E., Figer D. F., Gilbert A. M., Graham J, R., Larkin J. E., Levenson N. A., Wilcox M. k., 2000, ApJ, 533, L65

Walborn N. R., Bohlin R. C., 1996, PASP, 108, 477

Weymann R. J., et al. 1998, ApJ, 506, 1

Yee H. K., Ellingson E., Bechtold J., Carlberg R. G., Cuillandre J.–C., 1996, AJ, 111, 1783

This preprint was prepared with the AAS LaTeX macros v4.0.

Table 1: Journal of the observations

Date (day/month/year)	setup	seeing (″)	exp time (s)	airmass
13/03/00	R5200	0.6	5000	2.1
03/04/00	R5200	0.5	5650	2.1
26/04/00	R5200	0.6	5400	2.1
08/06/00	R5200	1.1	5650	2.15
10/06/00	R5200	0.4	5650	2.08
01/07/00	R5200	0.7	5650	2.32
total red arm			33000	
02/07/00	B4370	1.3	5400	2.08
04/07/00	B4370	0.6	5400	2.24
04/07/00	B4370	0.6	5400	2.09
05/07/00	B4370	0.4	5400	2.32
05/07/00	B4370	0.4	5400	2.07
26/07/00	B4370	0.7	5400	2.07
28/07/00	B4370	1.5	5400	2.07
02/08/00	B4370	0.7	5400	2.07
total blue arm			43200	

Table 2: Line parameters of the Lyα forest of cB58

#	λ_{obs} (Å)	z	$\log N_{\rm HI}$ ($\rm cm^{-2}$)	b ($\rm km\ s^{-1}$)
1	4158.75 ± 0.05	2.42095 ± 0.00004	14.90 ± 2.61	15 ± 13
2	4161.48 ± 0.07	2.42320 ± 0.00006	13.46 ± 0.19	14 ± 9
3	4174.00 ± 0.05	2.43350 ± 0.00004	14.38 ± 0.84	19 ± 10
4	4177.81 ± 0.08	2.43663 ± 0.00007	14.83 ± 2.47	14 ± 10
5	4179.07 ± 0.30	2.43767 ± 0.00025	13.99 ± 0.35	50 ± 47
6	4181.38 ± 0.64	2.43957 ± 0.00053	14.29 ± 0.17	132 ± 41
7	4192.76 ± 0.08	2.44893 ± 0.00007	13.96 ± 0.12	37 ± 8
8	4194.33 ± 0.09	2.45022 ± 0.00007	13.60 ± 0.14	23 ± 9
9	4197.30 ± 0.08	2.45266 ± 0.00007	13.47 ± 0.16	17 ± 11
10	4205.92 ± 0.19	2.45975 ± 0.00016	13.64 ± 0.14	57 ± 19
11	4208.54 ± 0.40	2.46191 ± 0.00033	13.73 ± 0.12	110 ± 37
12	4213.82 ± 0.10	2.46626 ± 0.00008	13.97 ± 0.10	46 ± 8
13	4216.01 ± 0.52	2.46805 ± 0.00043	13.51 ± 0.23	97 ± 67
14	4220.25 ± 0.06	2.47155 ± 0.00005	14.00 ± 0.38	20 ± 9
15	4243.77 ± 0.13	2.49089 ± 0.00011	13.43 ± 0.10	42 ± 13
16	4246.17 ± 0.04	2.49286 ± 0.00003	15.05 ± 0.49	54 ± 12
17	4249.05 ± 0.07	2.49524 ± 0.00006	14.06 ± 0.06	52 ± 6
18	4254.79 ± 0.23	2.49996 ± 0.00019	13.76 ± 0.10	92 ± 28
19	4257.21 ± 0.07	2.50195 ± 0.00006	13.95 ± 0.10	35 ± 7
20	4259.37 ± 0.17	2.50372 ± 0.00014	13.87 ± 0.08	80 ± 20
21	4277.07 ± 0.04	2.51828 ± 0.00003	14.08 ± 0.14	28 ± 5
22	4283.77 ± 0.03	2.52379 ± 0.00002	14.18 ± 0.19	26 ± 5
23	4288.09 ± 0.14	2.52734 ± 0.00012	13.68 ± 0.07	71 ± 13
24	4294.19 ± 0.22	2.53236 ± 0.00018	13.88 ± 0.10	98 ± 31
25	4296.58 ± 0.06	2.53433 ± 0.00005	13.82 ± 0.11	26 ± 7
26	4299.52 ± 0.06	2.53675 ± 0.00005	13.82 ± 0.56	11 ± 6
27	4301.15 ± 0.08	2.53809 ± 0.00007	14.71 ± 1.88	18 ± 13
28	4302.50 ± 0.13	2.53920 ± 0.00011	14.40 ± 0.18	40 ± 10
29	4309.53 ± 0.06	2.54498 ± 0.00005	13.47 ± 0.11	19 ± 5
30	4319.53 ± 0.02	2.55321 ± 0.00002	14.27 ± 2.07	12 ± 12

Table 2: – *Continued*

#	λ_{obs} (Å)	z	$\log N_{\rm HI}$ ($\rm cm^{-2}$)	b ($\rm km\ s^{-1}$)
31	4323.20 ± 0.04	2.55623 ± 0.00003	14.16 ± 1.73	8 ± 7
32	4329.14 ± 0.43	2.56112 ± 0.00035	15.50 ± 2.06	10 ± 11
33	4330.32 ± 0.47	2.56209 ± 0.00039	13.68 ± 0.12	119 ± 41
34	4334.54 ± 0.04	2.56556 ± 0.00003	15.17 ± 2.61	15 ± 9
35	4341.74 ± 0.05	2.57148 ± 0.00004	14.42 ± 0.13	49 ± 6
36	4356.25 ± 0.10	2.58342 ± 0.00008	13.26 ± 0.12	24 ± 12
37	4357.59 ± 0.05	2.58451 ± 0.00004	14.11 ± 0.10	31 ± 6
38	4359.11 ± 0.04	2.58577 ± 0.00003	15.66 ± 2.68	20 ± 12
39	4364.74 ± 0.02	2.59040 ± 0.00002	15.83 ± 1.77	15 ± 6
40	4374.26 ± 0.03	2.59823 ± 0.00002	15.97 ± 1.80	17 ± 6
41	4376.04 ± 0.12	2.59969 ± 0.00010	13.22 ± 0.15	24 ± 12
42	4378.29 ± 0.20	2.60154 ± 0.00016	13.45 ± 0.15	50 ± 20
43	4385.65 ± 0.11	2.60760 ± 0.00009	14.23 ± 0.15	53 ± 10
44	4387.92 ± 0.05	2.60946 ± 0.00004	14.57 ± 1.97	13 ± 13
45	4392.70 ± 0.04	2.61340 ± 0.00003	13.93 ± 0.11	24 ± 4
46	4394.66 ± 0.46	2.61501 ± 0.00038	13.34 ± 0.28	52 ± 36
47	4398.80 ± 0.03	2.61841 ± 0.00002	14.32 ± 0.20	28 ± 4
48	4400.91 ± 0.03	2.62015 ± 0.00002	14.44 ± 0.96	19 ± 9
49	4402.81 ± 0.06	2.62171 ± 0.00005	14.51 ± 0.31	35 ± 10
50	4404.96 ± 0.06	2.62349 ± 0.00005	15.45 ± 0.89	42 ± 13
51	4407.25 ± 0.07	2.62536 ± 0.00006	13.37 ± 0.09	23 ± 9
52	4410.55 ± 0.02	2.62808 ± 0.00002	15.09 ± 2.03	10 ± 7
53	4411.84 ± 0.14	2.62914 ± 0.00012	13.20 ± 0.12	36 ± 12
54	4414.48 ± 0.07	2.63131 ± 0.00006	14.05 ± 0.28	19 ± 8
55	4415.76 ± 0.20	2.63236 ± 0.00016	14.05 ± 0.18	52 ± 28
56	4416.76 ± 0.17	2.63319 ± 0.00014	14.45 ± 5.72	10 ± 13
57	4421.71 ± 0.21	2.63726 ± 0.00017	13.53 ± 0.12	64 ± 24
58	4426.66 ± 0.09	2.64133 ± 0.00007	14.68 ± 0.14	86 ± 16
59	4450.17 ± 0.14	2.66067 ± 0.00012	14.76 ± 0.11	93 ± 10
60	4453.99 ± 0.08	2.66381 ± 0.00007	13.62 ± 0.07	44 ± 8

Table 3: Absorption metal lines associated with cB58

#	ID	λ_{res} (Å)	λ_{obs} (Å)	z
1	NI	1134.165	4220.18	2.72095
2	NI	1134.415	4221.10	2.72095
3	NI	1134.980	4223.21	2.72095
4	NI	1134.165	4224.07	2.72438
5	NI	1134.415	4225.00	2.72438
6	NI	1134.165	4226.07	2.72615
7	NI	1134.415	4227.00	2.72615
8	NI	1134.980	4227.10	2.72438
9	NI	1134.980	4229.11	2.72615
10	FeII	1144.938	4260.94	2.72155
11	FeII	1144.938	4264.56	2.72471
12	FeII	1144.938	4267.25	2.72706
13	CIII	1175.7	4383.00	2.60542
14	SiII	1190.416	4429.98	2.72137
15	SiII	1190.416	4433.60	2.72441
16	SIiI	1190.416	4436.83	2.72713
17	SiII	1193.290	4440.67	2.72137
18	SiII	1193.290	4444.30	2.72441
19	SiII	1193.290	4447.54	2.72713
20	NI	1199.550	4463.47	2.72095
21	NI	1200.223	4465.97	2.72095
22	NI	1199.550	4467.58	2.72438
23	NI	1200.710	4467.78	2.72095
24	NI	1199.550	4469.70	2.72615
25	NI	1200.223	4470.09	2.72438
26	NI	1200.710	4471.90	2.72438
27	NI	1200.223	4472.21	2.72615
28	NI	1200.710	4474.02	2.72615
29	SiIII	1206.500	4486.72	2.71879
30	SiIII	1206.500	4489.75	2.72130
31	SiIII	1206.500	4493.58	2.72448
32	SiIII	1206.500	4497.28	2.72754
33	HI	1215.670	4527.36	2.72417

Table 4: Mean depression D_A in QSO sight lines

QSO	mag	z_{em}	FWHM (km s^{-1})	λ range (A)	$< z >$	Δz	D_A
J2233–606[a]	B17.5	2.238	7	3580–3900	2.07649	0.2632	0.118 ± 0.044
HE1347–2457[b]	R16.3	2.534	7	4050–4250	2.41376	0.1645	0.174 ± 0.025
GB1759+7539[c]	R16.5	3.05	7	4150–4348	2.49519	0.1629	0.212 ± 0.040
HS1946+7458[d]	V15.9	3.051	7.9	4170–4430	2.53714	0.2139	0.223 ± 0.023

[a] Cristiani & D'Odorico, 2000; [b] Kim et al., 2001b; [c] Outram et al., 1999; [d] Kirkman & Tytler, 1997.

Table 5: Mean depression in different intervals of cB58 and QSO sight lines.

		D_A			
λ range	$< z >$	cB58	GB1759+7539	HE1347–2457	HS1946+7458
4050–4150	2.3315	–	–	0.184 (0.159–0.208)	–
4150–4250	2.4549	0.215 (0.174–0.253)	0.234 (0.193–0.270)	0.165 (0.138–0.189)	0.219 (0.195–0.242)[a]
4250–4348	2.5363	0.232 (0.192–0.269)	0.189 (0.146–0.228)	–	0.240 (0.216–0.262)
4348–4430	2.6104	0.358 (0.325–0.389)	–	–	0.206 (0.182–0.229)

[a]This value is calculated in the wavelength range 4170–4250 Å, at $< z >= 2.4631$.

Table 6: Number of Lyα clouds in cB58 and different QSO sight lines

			Number of Lyα clouds ($\log N_{\rm HI} \geq 13.7$)			
λ range	$< z >$	Δz	cB58	GB1759+7539	HE1347–2457	HS1946+7658
4050–4150	2.3315	0.0823	–	–	10 (6.9–14.3)	–
4150–4250	2.4549	0.0823	11 (7.7–15.4)	12 (8.6–16.6)	11 (7.7–15.4)	10 (6.9–14.3)[a]
4250–4348	2.5363	0.0806	15 (11.2–20.0)	7 (4.4–10.8)	–	12 (8.6–16.6)
4348–4430	2.6104	0.0675	16 (12.1–21.1)	–	–	9 (6.1–13.1)

[a]This value is calculated rescaling from the value obtained in the wavelength range 4170–4250 Å, at $< z >= 2.4631$.

Table 7: Number of Lyα clouds in cB58 and different QSO sight lines

			Number of Lyα clouds ($\log N_{\rm HI} \geq 14.0$)			
λ range	$< z >$	Δz	cB58	GB1759+7539	HE1347–2457	HS1946+7658
4050–4150	2.3315	0.0823	–	–	8 (5.2–11.9)	–
4150–4250	2.4549	0.0823	7 (4.4–10.8)	9 (6.1–13.1)	5 (2.9–8.4)	6 (3.6–9.6)[a]
4250–4348	2.5363	0.0806	9 (6.1–13.1)	4 (2.1–7.2)	–	6 (3.6–9.6)
4348–4430	2.6104	0.0675	15 (11.2–20.0)	–	–	2 (0.7–4.6)

[a]This value is calculated rescaling from the value obtained in the wavelength range 4170–4250 Å, at $< z >= 2.46311$.

Fig. 1.— The Lyman–α forest of cB58 (thick line) with the fitted Voigt profiles (thin smooth line). The spectrum of the noise per resolution is also shown. Arrows indicate the position of metal and Lyα lines associated with the galaxy itself. Large and small ticks mark Lyα clouds with HI column density $N_{\rm HI} \geq 10^{13.7}$ cm^{-2} and $N_{\rm HI} < 10^{13.7}$ cm^{-2}, respectively.

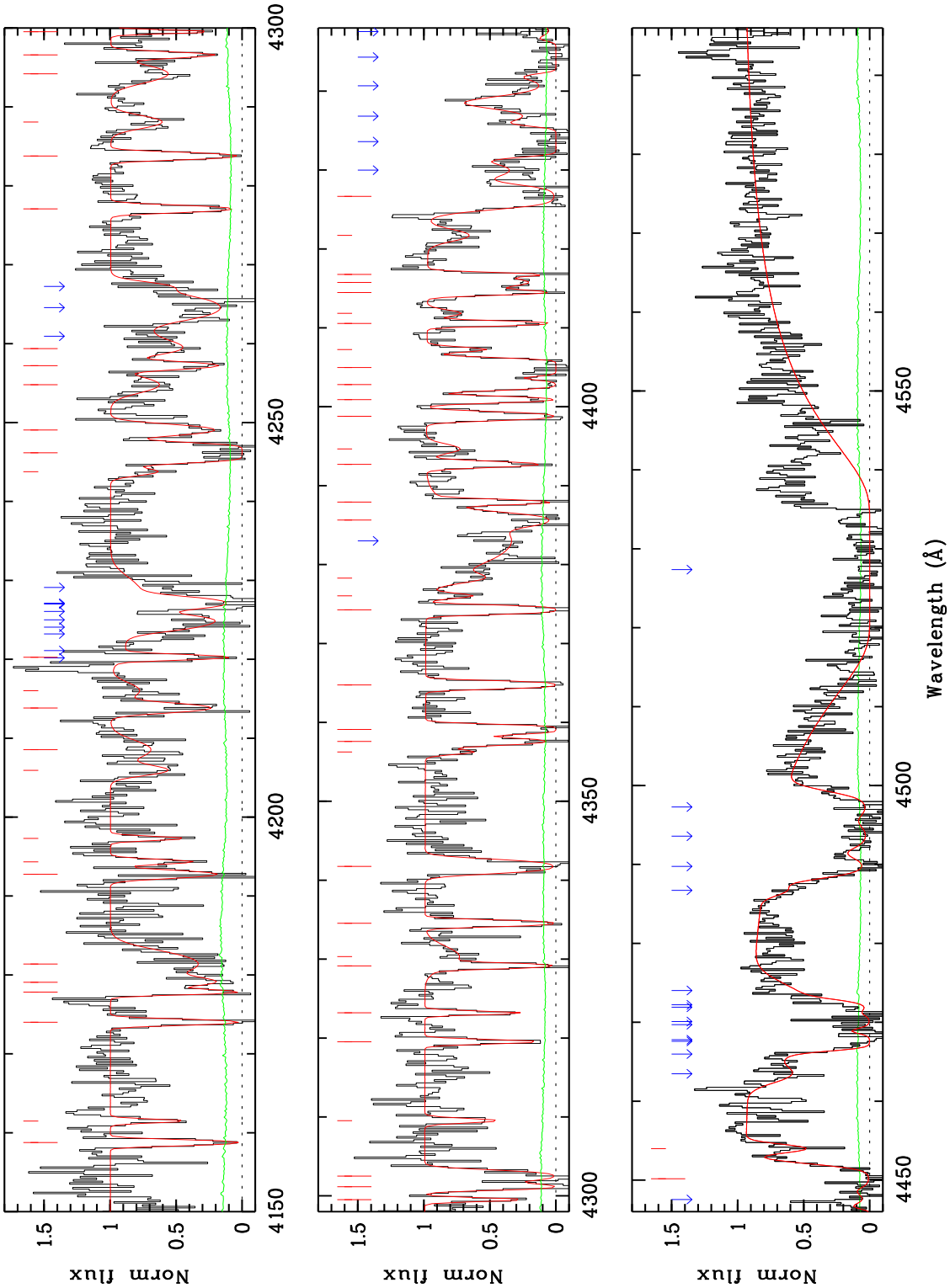


Fig. 2.— The Lyman–α forest of cB58 (upper spectrum) compared with QSO sight lines of HS1946+7458, HE1347–2457 and GB1759+7539.

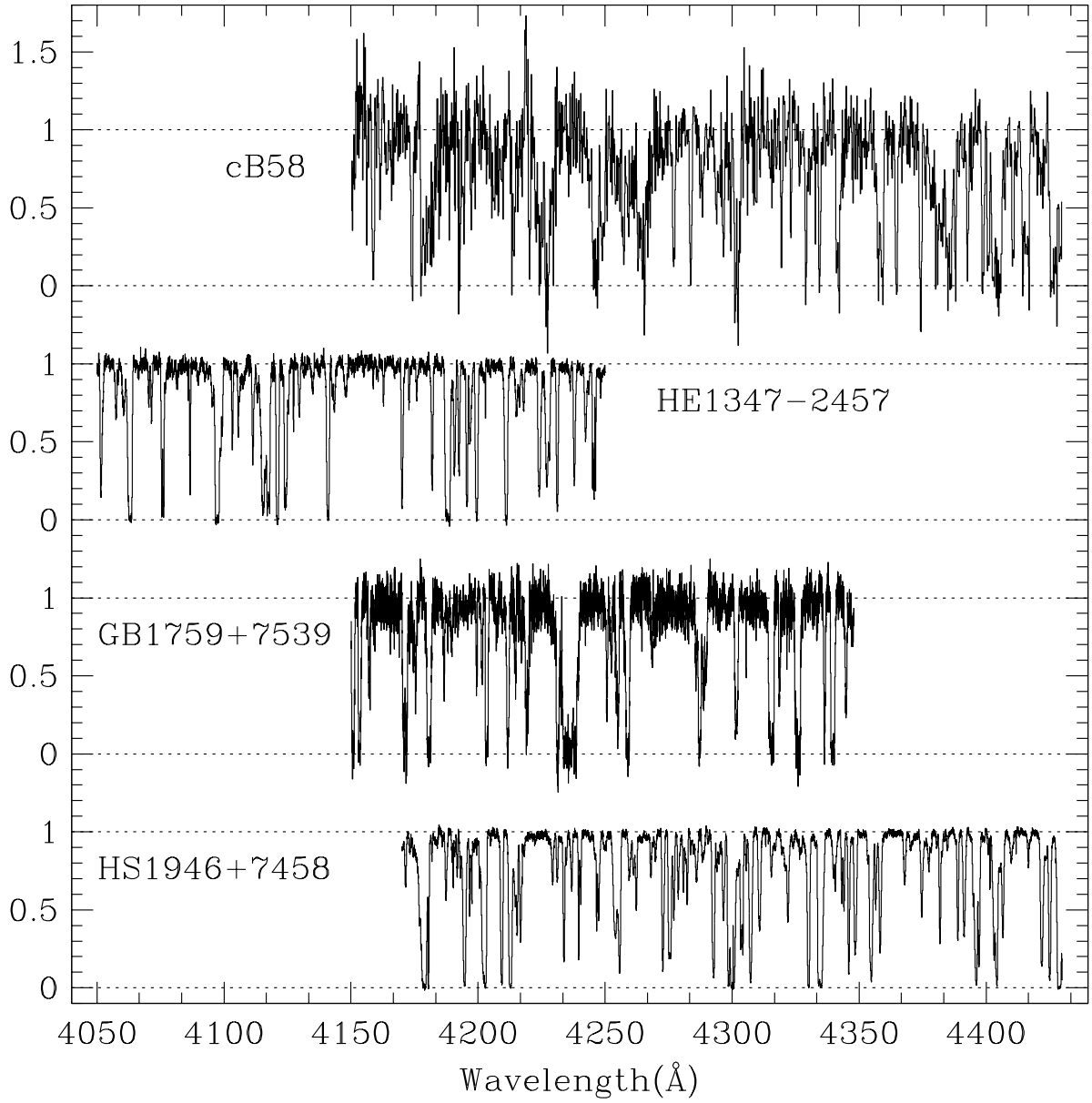


Fig. 3.— Mean depression D_A as a function of mean redshifts in cB58 (open circle), and in different QSO lines of sight. Triangles are for J2233–606, HE1347–2457, GB1759+7539, and HS1946+7458, from the lowest to the highest redshift, respectively. Squares are from Keck/HIRES and VLT/UVES high resolution data (Kim et al., 2001a). The solid and dashed curves are the best fit to D_A $\pm 1\sigma$, respectively ($D_A = 1 - \exp(-0.003 \times (1+z)^{3.43\pm0.17})$), obtained by Kim et al. (2001a) in the redshift interval $1.6 < z < 4.3$.

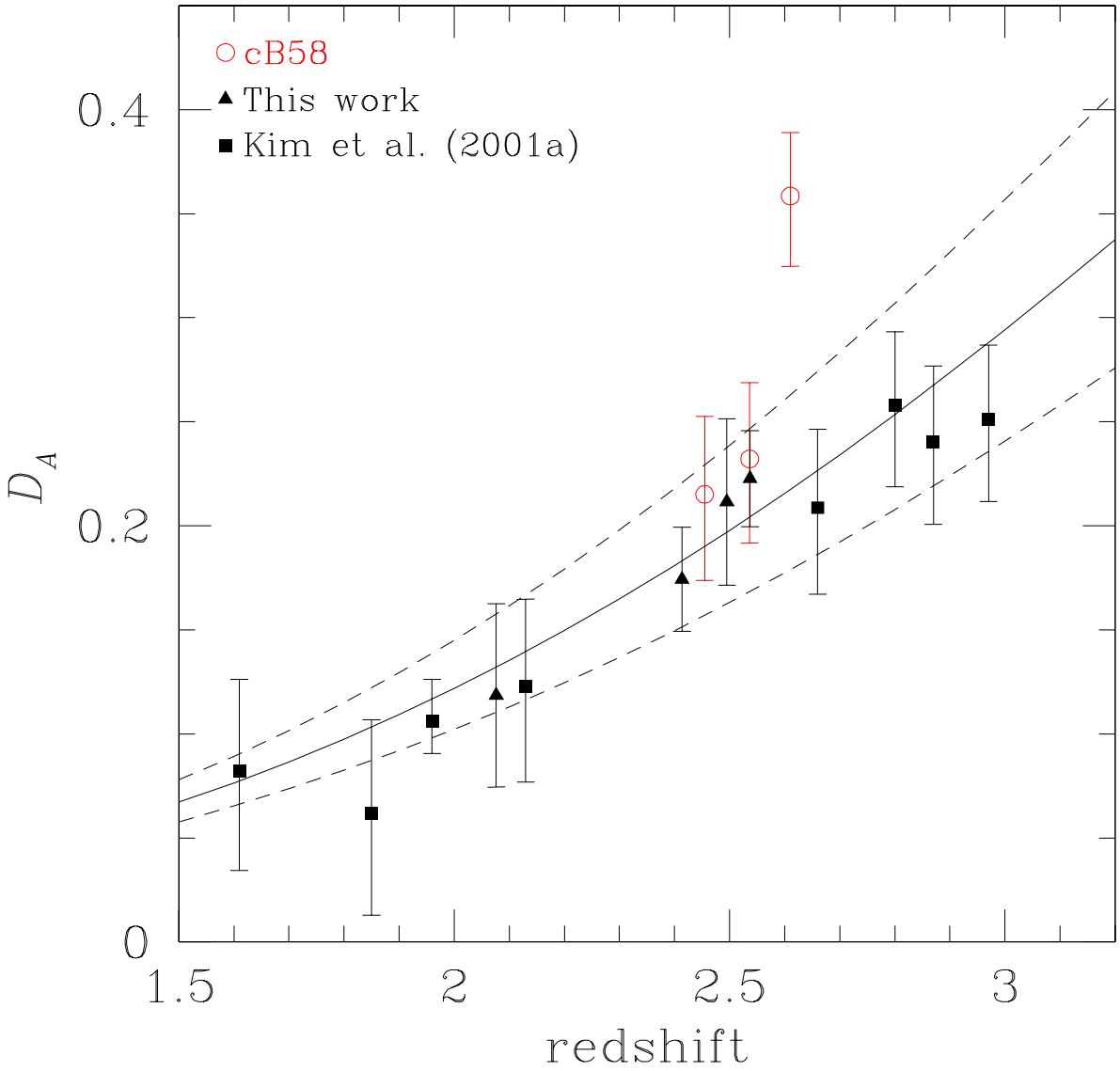


Fig. 4.— Spectrum of cB58 (lower spectrum) compared with that of the nearby dwarf starburst galaxy NGC1705 at redshift $v = +569$ km s^{-1} (upper spectrum, Heckman et al., 2001). Upper and lower x–axis scales give the rest frame and observed wavelength range. Vertical ticks in mark the ISM multiplets of NI(1134) and FeII(1144), and the stellar lines SiIV(1122), SiIV(1128) and CIII(1176). The non marked features blushifted by ~ 600 km s^{-1} in NGC1705 are absorption lines of the Milky Way.

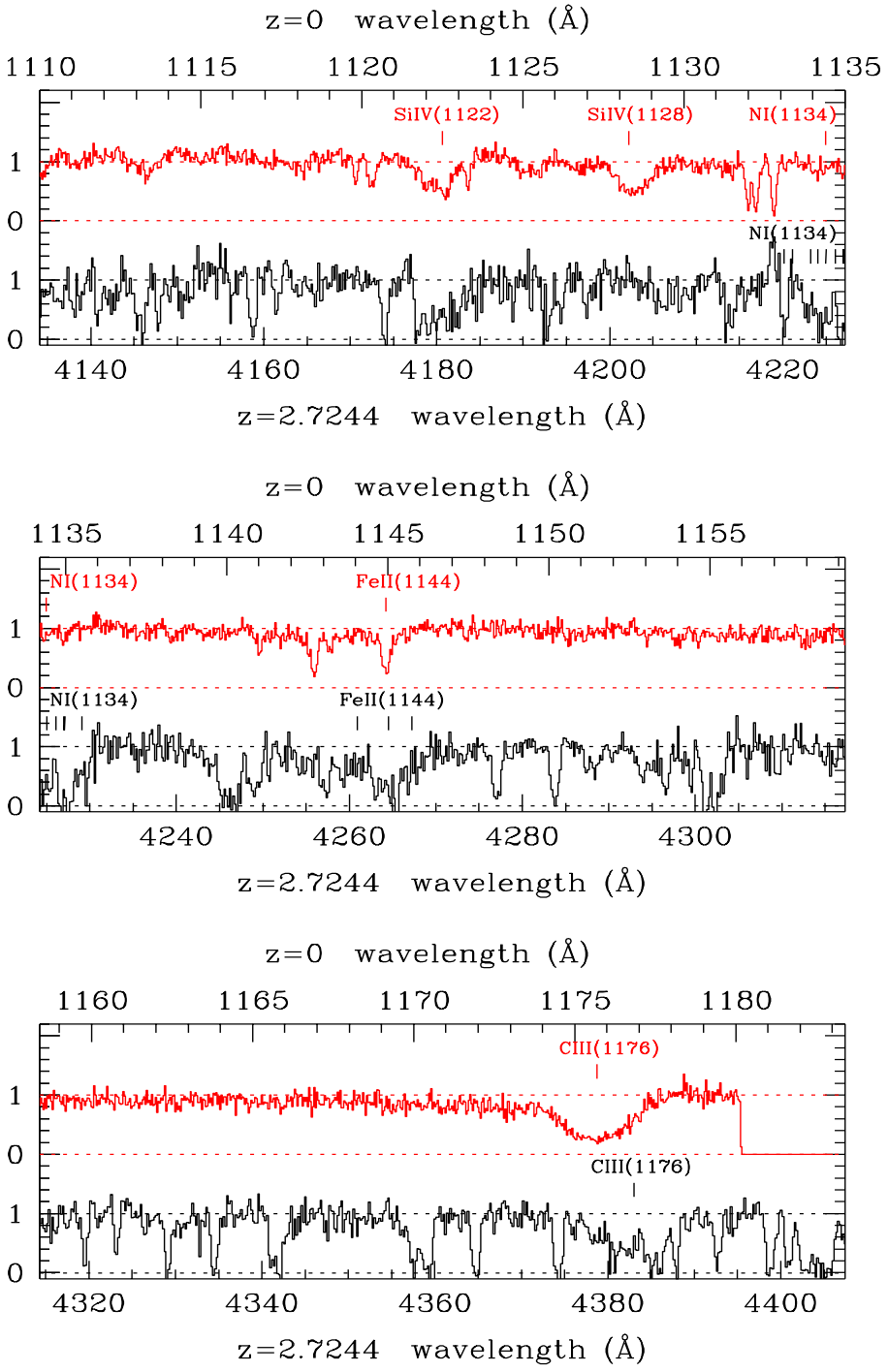


Fig. 5.— Number density evolution of Lyα clouds for HI column density lines with $N_{\rm HI} \geq 10^{14}$ atoms cm^{-2}. The straight line is the best fit for QSO forests with $z \geq 2.3$.

